ACS NANO

www.acsnano.org

ARTICLE

Mesoscopic Morphologies in Frustrated ABC Bottlebrush Block Terpolymers

Shuquan Cui, Elizabeth A. Murphy, Subrata Santra, Frank S. Bates,* and Timothy P. Lodge*

Cite This: *ACS Nano* 2025, 19, 1211−1221

Read Online

ACCESS | Metrics & More | Article Recommendations | Supporting Information

ABSTRACT: Bottlebrush block polymers, characterized by densely grafted side chains extending from a backbone, have recently garnered significant attention. A particularly attractive feature is the accessibility of ordered morphologies with domain spacings exceeding several hundred nanometers, a capability that is challenging to achieve with linear polymers. These large morphologies make bottlebrush block polymers promising for various applications, such as photonic crystals. However, the structures observed in AB diblock bottlebrushes are generally limited to simple lamellae and cylindrical phases, which restricts their use in many applications. In this study, we synthesized a library of 50 ABC bottlebrush triblock terpolymers, poly(DL-lactide)-*b*-poly(ethylene-*alt*-propylene)-*b*-polystyrene (PLA-PEP-PS), spanning a wide range of compositions using ring-opening metathesis polymerization (ROMP) of norbornene-functionalized macromonomers. This constitutes a frustrated system, in that the mandatory internal interfaces (PLA/PEP and PEP/PS) have larger interfacial energies than PLA/PS. We systematically explored phase behavior using small-angle X-ray scattering (SAXS) and transmission electron microscopy (TEM). Morphological characterization revealed a series of intriguing mesoscopic structures, including layered microstructures, core-shell hexagonally packed cylinders (CSHEX, plane group *p6mm*), alternating tetragonally packed cylinders (ATET, plane group *p4mm*), and rectangular centered cylinders-in-undulating-lamellae (RCCUL, plane group *c2mm*). Adjustments in molecular weight resulted in a wide range of unit cell dimensions (exemplified by RCCUL), from 40 nm to over 130 nm. This work demonstrates that multiblock bottlebrushes offer promising opportunities for developing materials with diverse structures and a broad range of domain dimensions.

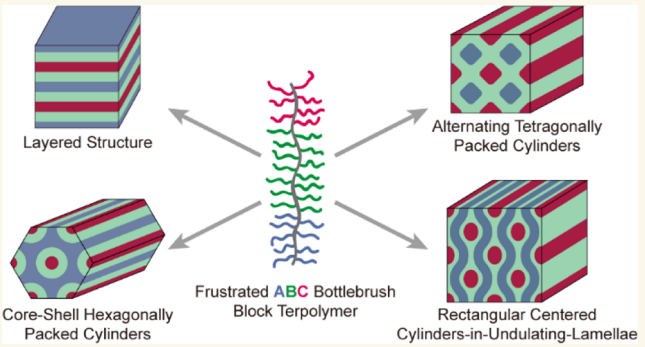

KEYWORDS: *bottlebrush, block copolymer, self-assembly, phase portrait, mesoscopic morphology*

INTRODUCTION

Block copolymers can spontaneously assemble into a plethora of mesoscopic ordered morphologies with typical domain spacings of 10−50 nm,[1] finding applications in diverse fields, such as thermoplastic elastomers,[2,3] drug delivery,[4,5] nanopatterning,[6,7] and porous materials.[8−10] The ordered phase morphology is determined by a trade-off between the interfacial tension between microphase-separated domains and the entropic cost of chain stretching needed to achieve uniform space-filling.[11] This balance is primarily influenced by molecular parameters. For example, the formation of the equilibrium phase in linear flexible AB diblock copolymers, the simplest architecture, is governed by three key independent parameters: (*i*) the total volumetric degree of polymerization N (proportional to molecular weight), (*ii*) the Flory−Huggins segment−segment interaction parameter χ_{AB}, and (*iii*) the volume fraction f_A of block A, where $f_B = 1 - f_A$.[12,13] In the phase portrait for linear diblocks with f_A as the abscissa and segregation strength ($\chi_{AB}N$) as the ordinate, the sequence of phases lamellae (LAM) − gyroid (GYR) − hexagonally packed cylinders (HEX) − spheres (S) − disorder (DIS) is obtained as f_A increases ($f_A \rightarrow 1$) or decreases ($f_A \rightarrow 0$) from the symmetric condition $f_A = 0.5$.[14]

Addition of a third block C leads to linear ABC triblock terpolymers, exposing new opportunities for materials with unconventional morphologies.[15−17] In contrast to AB diblocks, the phase behavior of ABC triblocks is dictated by six independent parameters: (*i*) N, (*ii*) f_A and f_B ($f_C = 1 - f_A - f_B$), and (*iii*) χ_{AB}, χ_{BC}, and χ_{AC}.[16] Based on the relative interaction strengths, ABC triblocks have been classified as either nonfrustrated (χ_{AC} is greater than both χ_{AB} and χ_{BC}) or

Received: September 23, 2024
Revised: December 8, 2024
Accepted: December 16, 2024
Published: January 6, 2025

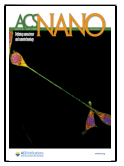

Scheme 1. Synthesis Route to Frustrated PLA-PEP-PS Bottlebrush Block Terpolymers Using Ring-Opening Metathesis Polymerization (ROMP)

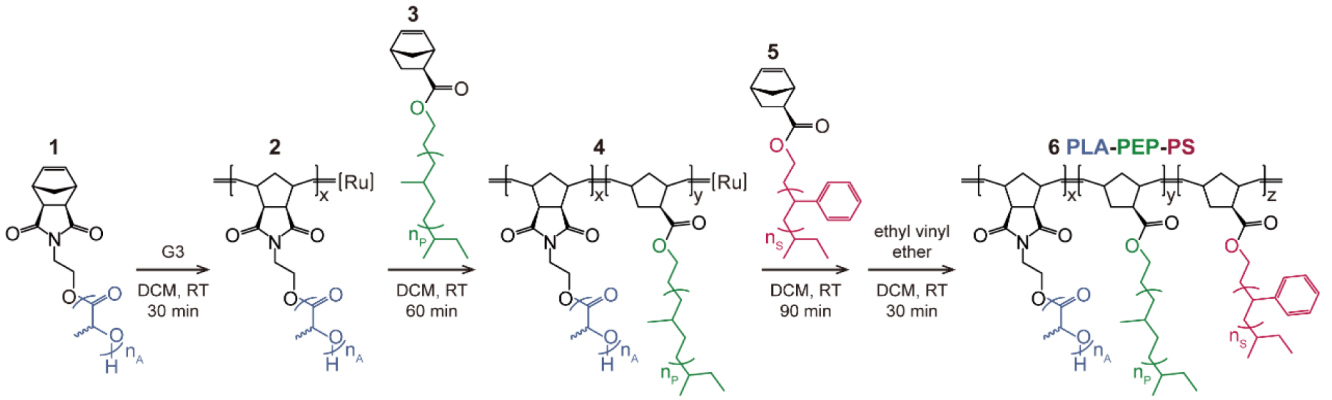

frustrated (χ_{AC} is smaller than either χ_{AB} or χ_{BC}) systems.[18] The relative interaction strengths, influencing the enthalpic preference of interfaces, together with the block connectivity, lead to distinguishable phase behavior in ABC block terpolymers. For example, the nonfrustrated system, which does not favor A/C contacts, mainly forms structures resembling those in AB diblock copolymers. These include core-shell configurations (core-shell spheres, cylinders, GYR, LAM (three-color LAM)), and alternating structures (alternating spheres, cylinders, GYR).[18,19] In contrast, frustrated systems (especially systems where χ_{AC} is smallest) tend to favor morphologies including A/C contacts, such as X-in-Y structures (e.g., cylinders-in-lamellae or spheres-in-lamellae).[20−22]

Recently, bottlebrush polymers, characterized by densely grafted side chains on a backbone, have garnered significant attention due to their distinct structural and dynamic properties in comparison to linear counterparts.[23,24] Among the various types of bottlebrush polymers—such as core-shell,[25] Janus,[26,27] and statistical bottlebrushes;[28] the bottlebrush block polymer is particularly attractive owing to its ability to form large-scale morphologies.[29] The densely grafted side chains elongate the molecular conformations and strongly couple the domain spacing (d) to the backbone degree of polymerization (N_{bb}) where $d \sim N_{bb}^{0.8-0.9}$.[30] Here the exponent is larger than the value associated with linear systems, where $d \sim N^{0.5-0.67}$.[31] Furthermore, the relaxation kinetics of bottlebrush block polymers are significantly faster due to a large cross-sectional area, which minimizes the chain entanglement, implicated in slow ordering kinetics for high molecular weight linear polymers.[32] These two aspects together contribute to large domain spacings reaching up to several hundred nanometers, making the bottlebrush block polymers promising in applications such as photonic crystals requiring dimensions approaching the wavelength of visible light.[33,34] However, the morphologies found in AB bottlebrush diblock copolymers are so far limited to the LAM and HEX phases.[35,36] One possible reason is that the more congested architecture of the bottlebrush makes it more difficult to fill the intricate space imposed by the complex structures.

In recent work, we discovered that extending the AB bottlebrush diblock copolymer to a nonfrustrated ABC bottlebrush triblock terpolymer resulted in complex morphologies, including a core-shell GYR, and the unique 2D morphology cylinders-in-undulating-lamellae (CUL, plane group $p2$).[37,38] These findings indicate that bottlebrush triblock terpolymers offer opportunities to access new materials, which encouraged us to further explore their phase behavior. In this study, we systematically investigated the phase behavior of poly(DL-lactide)-*b*-poly(ethylene-*alt*-propylene)-*b*-polystyrene (PLA-PEP-PS, $\chi_{PLA-PEP} > \chi_{PLA-PS} > \chi_{PEP-PS}$), synthesized by ring-opening metathesis polymerization (ROMP, Scheme 1). Morphological characterization demonstrated a variety of mesoscopic morphologies, including several layered structures, core-shell hexagonally packed cylinders (CSHEX, plane group *p6mm*), alternating tetragonally packed cylinders (ATET, plane group *p4mm*), and an unprecedented morphology, rectangular centered cylinders-in-undulating-lamellae (RCCUL, plane group *c2mm*). Adjustments in molecular weight resulted in a wide range of unit cell dimensions, exemplified by the RCCUL morphology, spanning from 40 nm to over 130 nm. Our findings further demonstrate that ABC bottlebrush block terpolymers can generate a diverse array of structures with various symmetries and dimensions.

RESULTS

Synthesis and Characterization of ABC Bottlebrush Triblock Terpolymers. Frustrated PLA-PEP-PS bottlebrush triblock terpolymers were synthesized by ROMP of norbornene-functionalized macromonomers, PLA (MM_A, number-average molecular weight M_n = 1780 g/mol, molar-mass dispersity $Đ$ = 1.13), PEP (MM_P, M_n = 1290 g/mol, $Đ$ = 1.11), and PS (MM_S, M_n = 1240 g/mol, $Đ$ = 1.14) with Grubbs third generation catalyst (G3), following the procedure (Scheme 1) reported in our previous work.[37,38] Specific details regarding polymer characterization are provided in the Experimental Methods and Figures S1−S3. A library of PLA-PEP-PS triblocks along an f_{PLA}/f_{PEP} isopleth in the ternary phase portrait (i.e., constant f_{PLA}/f_{PEP} but varying f_{PS}) can be rapidly generated by extending a parent PLA-PEP diblock with differing amounts of MM_S. Typical size exclusion chromatography (SEC) profiles of bottlebrushes derived from a specific diblock (f_{PLA}/f_{PEP} = 2.33) are depicted in Figure 1. Each bottlebrush polymer exhibited a narrow molecular weight distribution with $Đ$ usually less than 1.2. The molecular parameters of all bottlebrushes are listed in Table 1. Our sample nomenclature, superscript and subscript after each block label, reflects the volume fraction f and the backbone degree of polymerization N_{bb} of each block, respectively.

Phase Behavior of ABC Bottlebrush Triblock Terpolymers. The bulk morphologies of all polymers were

https://doi.org/10.1021/acsnano.4c13416
ACS Nano 2025, 19, 1211−1221

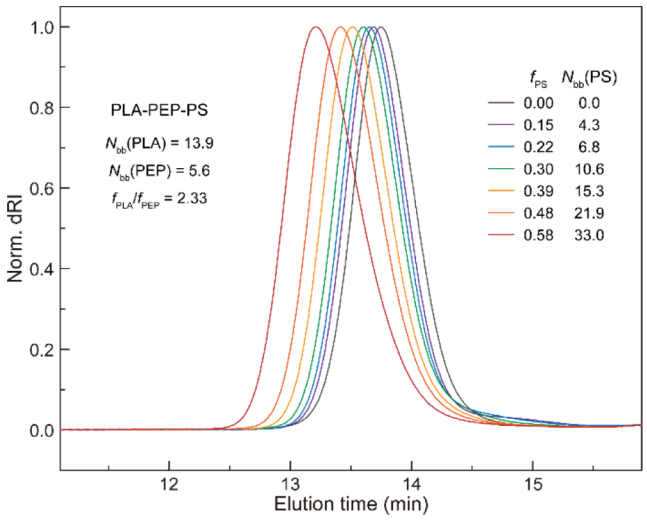

Figure 1. Typical SEC profiles of PLA-PEP-PS bottlebrush triblock polymers obtained from a diblock with f_{PLA}/f_{PEP} = 2.33.

characterized by small-angle X-ray scattering (SAXS), supplemented by transmission electron microscopy (TEM). Unless otherwise noted, polymer samples were freeze-dried and then annealed at 150 °C (well above the glass-transition temperatures of all blocks, Figure S3) under vacuum for 24 h. SEC profiles (Figure S2) confirmed that neither cross-linking nor degradation occurred during the annealing process. SAXS measurements were conducted at a target temperature (usually 80 °C) after a 10 min equilibration. TEM images were collected from ultrathin polymer sections (~70 nm) prepared by cryo-microtoming at around −70 °C, followed by reaction with the vapor from an aqueous RuO_4 solution for 4 min, resulting in unstained PEP domains (white), slightly stained PLA domains (gray), and strongly stained PS domains (black). Details of the characterization can be found in the Experimental Methods.

Since complex phases are more likely to appear in the weak segregation region (low χN),[41] we initiated the investigation using low molecular weight samples with N_{bb}(PLA) + N_{bb}(PEP) ≈ 20. In PLA-PEP diblocks (f_{PS} = 0.0), only two ordered morphologies were found, LAM and HEX (Figure S4). These results are consistent with those reported in previous works.[35,36,42] In contrast, addition of the third PS block (PLA-PEP-PS triblocks with f_{PS} > 0.0) led to a rich library of mesoscopic ordered morphologies (see the ternary phase portrait in Figure 2), including four layered structures, LAM, defective LAM (DLAM), modulated layer (LAY_M), and two separate LAM phases (2LAM), and three cylinder-containing morphologies, core-shell hexagonally packed cylinders (CSHEX, plane group *p6mm*), alternating tetragonally packed cylinders (ATET, plane group *p4mm*), and a unique phase, rectangular centered cylinders-in-undulating-lamellae (RCCUL, plane group *c2mm*). Numerous samples displayed coexisting phases (LAM plus a cylinder-containing morphology). This phenomenon has been found previously,[43,44] although the underlying mechanism remains elusive. It should be noted that, when naming the layered phases, we did not clearly distinguish between two-color layers (formed by PLA-PEP diblocks or PLA-PEP-PS triblocks with mixed blocks) and three-color layers (formed by PLA-PEP-PS triblocks with three distinct domains).

Layered Structures. The LAM phase was identified based on sharp diffraction peaks appearing in the SAXS patterns at q/q^* = 1, 2, 3,⋯, where q^* identifies the position of the first reflection (Figure 3). SAXS patterns of other layered structures, DLAM, LAY_M, and 2LAM, also produced lamellar-like peaks along with additional (usually broader) peaks. All layered structures identified by SAXS were confirmed using TEM, and the details of the analyses are provided in the Figures S5−S10. Such layered structures are prevalent in the low molecular weight PLA-PEP-PS bottlebrush block terpolymers: the pure layered structures occurred in both low-f_{PS} (f_{PS} < 0.11) and high-f_{PS} (f_{PS} > 0.35) regions, separated by the medium-f_{PS} (0.11 < f_{PS} < 0.35) region, where cylinder-containing morphologies and layered phases coexisted (Figure 2).

The domain spacing of the layered structures was calculated based on $d = 2\pi/q^*$. Remarkably, for PLA-PEP-PS bottlebrush triblocks derived from the same parent PLA-PEP diblock (itself synthesized in a single batch), the domain spacing evolved nonmonotonically with N_{bb}, with a distinct gap appearing approximately in the compositional region where coexisting morphologies were present (Figure 4A). The results show that the domain spacing scales approximately as $d \sim N_{bb}^{-0.71\pm0.04}$ (R^2 = 0.99) and $d \sim N_{bb}^{0.75\pm0.02}$ (R^2 = 0.99) before and after the coexisting region, respectively, as shown in Figure 4A. We speculate that this counterintuitive phenomenon originates from the specific polymer packing shown in Figure 4B, and is a reflection of a two-color layer to three-color layer transition with increasing f_{PS}, which is further explored in the Discussion section.

Core-Shell Hexagonally Packed Cylinders (CSHEX). A core-shell version of the HEX phase (plane group *p6mm* based on the SAXS pattern, Figure 5A) was found in the PLA-rich region with 0.50 < f_{PLA} < 0.60, 0.16 < f_{PEP} < 0.34, and 0.13 < f_{PS} < 0.24, coexisting with LAM (Figure 2). A SAXS pattern as well as a TEM image from a representative CSHEX sample is shown in Figure 5. As revealed in the TEM image, white PEP domains form a shell surrounding black PS cylinders immersed in a gray PLA matrix. Distortion of the unit cell from a regular hexagon symmetry (Figure 5B) is likely due to either sections being sliced at an oblique angle or shear deformation occurring during sample preparation. A similar modest deviation in unit cell geometry was also observed in our earlier work.[38]

Alternating Tetragonally Packed Cylinders (ATET). Figure 6A displays a SAXS pattern with *p4mm* symmetry and a TEM image (Figure 6B) that confirms alternating tetragonally packed cylinders (ATET) with PLA and PS as the gray and black cylinders, respectively, and PEP as the white matrix. This tetragonal phase appears approximately in the PEP-rich region with 0.22 < f_{PLA} < 0.34, 0.32 < f_{PEP} < 0.58, and 0.14 < f_{PS} < 0.35 (Figure 2). The small extra low-q peak in Figure 6A (indicated by the hollow diamond) is attributed to lattice defects, which are identified by TEM in Figure S11.

Rectangular Centered Cylinders-in-Undulating-Lamellae (RCCUL). An extraordinary RCCUL phase with *c2mm* symmetry was observed in the region with $f_{PLA} \approx f_{PEP}$ (0.34 < f_{PLA} < 0.49, 0.31 < f_{PEP} < 0.52, and 0.11 < f_{PS} < 0.20), bracketed by CSHEX and ATET (Figure 2). Combining SAXS indexing (Figure 7A) and TEM visualization (Figure 7B) leads to an RCCUL phase with unit cell parameters $a = b$. Similar to the TEM image of CSHEX (Figure 5B), a small deviation of the unit cell angle from 90° (less than 10°) is observed in Figure 7B, again attributed to thin sections sliced at an oblique

https://doi.org/10.1021/acsnano.4c13416
ACS Nano 2025, 19, 1211−1221

Table 1. Molecular Parameters for the Bottlebrush Block Polymers

ID[a]	f_A[b]	f_B[b]	f_C[b]	M_n (kg/mol)[c]	$Đ$[d]
$PLA^{0.79}_{16.3}$-$PEP^{0.21}_{4.2}$	0.79	0.21	0.00	34.3	1.12
$PLA^{0.67}_{16.3}$-$PEP^{0.18}_{4.2}$-$PS^{0.14}_{4.4}$	0.67	0.18	0.14	39.5	1.18
$PLA^{0.60}_{16.3}$-$PEP^{0.16}_{4.2}$-$PS^{0.24}_{8.1}$	0.60	0.16	0.24	43.9	1.15
$PLA^{0.52}_{16.3}$-$PEP^{0.14}_{4.2}$-$PS^{0.34}_{13.3}$	0.52	0.14	0.34	50.2	1.17
$PLA^{0.43}_{16.3}$-$PEP^{0.12}_{4.2}$-$PS^{0.46}_{21.5}$	0.43	0.12	0.46	60.3	1.16
$PLA^{0.32}_{16.3}$-$PEP^{0.09}_{4.2}$-$PS^{0.59}_{36.8}$	0.32	0.09	0.59	79.4	1.19
$PLA^{0.70}_{13.9}$-$PEP^{0.30}_{5.6}$	0.70	0.30	0.00	32.0	1.11
$PLA^{0.60}_{13.9}$-$PEP^{0.26}_{5.6}$-$PS^{0.15}_{4.3}$	0.60	0.26	0.15	37.2	1.15
$PLA^{0.55}_{13.9}$-$PEP^{0.24}_{5.6}$-$PS^{0.22}_{6.8}$	0.55	0.24	0.22	40.1	1.13
$PLA^{0.49}_{13.9}$-$PEP^{0.21}_{5.6}$-$PS^{0.30}_{10.6}$	0.49	0.21	0.30	44.9	1.13
$PLA^{0.43}_{13.9}$-$PEP^{0.18}_{5.6}$-$PS^{0.39}_{15.3}$	0.43	0.18	0.39	50.7	1.13
$PLA^{0.37}_{13.9}$-$PEP^{0.16}_{5.6}$-$PS^{0.48}_{21.9}$	0.37	0.16	0.48	59.0	1.14
$PLA^{0.29}_{13.9}$-$PEP^{0.13}_{5.6}$-$PS^{0.58}_{33.0}$	0.29	0.13	0.58	72.9	1.17
$PLA^{0.61}_{10.8}$-$PEP^{0.39}_{6.6}$	0.61	0.39	0.00	27.7	1.11
$PLA^{0.52}_{10.8}$-$PEP^{0.34}_{6.6}$-$PS^{0.14}_{3.4}$	0.52	0.34	0.14	31.9	1.10
$PLA^{0.50}_{10.8}$-$PEP^{0.33}_{6.6}$-$PS^{0.17}_{4.4}$	0.50	0.33	0.17	33.1	1.10
$PLA^{0.48}_{10.8}$-$PEP^{0.31}_{6.6}$-$PS^{0.21}_{5.6}$	0.48	0.31	0.21	34.6	1.13
$PLA^{0.42}_{10.8}$-$PEP^{0.27}_{6.6}$-$PS^{0.31}_{9.4}$	0.42	0.27	0.31	39.3	1.14
$PLA^{0.36}_{10.8}$-$PEP^{0.24}_{6.6}$-$PS^{0.40}_{14.2}$	0.36	0.24	0.40	45.4	1.13
$PLA^{0.51}_{9.4}$-$PEP^{0.49}_{8.6}$	0.51	0.49	0.00	27.8	1.13
$PLA^{0.48}_{9.4}$-$PEP^{0.47}_{8.6}$-$PS^{0.05}_{1.2}$	0.48	0.47	0.05	29.3	1.13
$PLA^{0.47}_{9.4}$-$PEP^{0.45}_{8.6}$-$PS^{0.08}_{1.9}$	0.47	0.45	0.08	30.2	1.11
$PLA^{0.45}_{9.4}$-$PEP^{0.44}_{8.6}$-$PS^{0.11}_{2.7}$	0.45	0.44	0.11	31.3	1.14
$PLA^{0.43}_{9.4}$-$PEP^{0.42}_{8.6}$-$PS^{0.15}_{3.8}$	0.43	0.42	0.15	32.6	1.15
$PLA^{0.41}_{9.4}$-$PEP^{0.40}_{8.6}$-$PS^{0.19}_{5.2}$	0.41	0.40	0.19	34.4	1.15
$PLA^{0.38}_{9.4}$-$PEP^{0.37}_{8.6}$-$PS^{0.25}_{7.3}$	0.38	0.37	0.25	37.1	1.15
$PLA^{0.51}_{10.3}$-$PEP^{0.49}_{9.3}$	0.51	0.49	0.00	30.4	1.12
$PLA^{0.43}_{10.3}$-$PEP^{0.42}_{9.3}$-$PS^{0.15}_{4.2}$	0.43	0.42	0.15	35.7	1.14
$PLA^{0.43}_{10.3}$-$PEP^{0.41}_{9.3}$-$PS^{0.16}_{4.7}$	0.43	0.41	0.16	36.3	1.14
$PLA^{0.33}_{10.3}$-$PEP^{0.32}_{9.3}$-$PS^{0.35}_{12.5}$	0.33	0.32	0.35	46.3	1.14
$PLA^{0.23}_{10.3}$-$PEP^{0.22}_{9.3}$-$PS^{0.55}_{28.6}$	0.23	0.22	0.55	66.8	1.15
$PLA^{0.41}_{11.5}$-$PEP^{0.59}_{15.3}$	0.41	0.59	0.00	40.2	1.13
$PLA^{0.36}_{11.5}$-$PEP^{0.51}_{15.3}$-$PS^{0.12}_{4.5}$	0.36	0.51	0.12	46.1	1.15
$PLA^{0.35}_{11.5}$-$PEP^{0.49}_{15.3}$-$PS^{0.16}_{6.0}$	0.35	0.49	0.16	48.1	1.16
$PLA^{0.33}_{11.5}$-$PEP^{0.47}_{15.3}$-$PS^{0.20}_{7.7}$	0.33	0.47	0.20	50.3	1.16
$PLA^{0.28}_{11.5}$-$PEP^{0.40}_{15.3}$-$PS^{0.32}_{14.7}$	0.28	0.40	0.32	59.4	1.15
$PLA^{0.32}_{8.2}$-$PEP^{0.68}_{16.3}$	0.32	0.68	0.00	35.7	1.12
$PLA^{0.27}_{8.2}$-$PEP^{0.58}_{16.3}$-$PS^{0.15}_{5.0}$	0.27	0.58	0.15	42.5	1.15
$PLA^{0.26}_{8.2}$-$PEP^{0.55}_{16.3}$-$PS^{0.19}_{6.7}$	0.26	0.55	0.19	44.8	1.15
$PLA^{0.23}_{8.2}$-$PEP^{0.48}_{16.3}$-$PS^{0.30}_{12.1}$	0.23	0.48	0.30	51.9	1.14
$PLA^{0.18}_{8.2}$-$PEP^{0.37}_{16.3}$-$PS^{0.45}_{23.8}$	0.18	0.37	0.45	67.3	1.14
$PLA^{0.20}_{3.8}$-$PEP^{0.80}_{14.5}$	0.20	0.80	0.00	25.4	1.14
$PLA^{0.17}_{3.8}$-$PEP^{0.69}_{14.5}$-$PS^{0.14}_{3.3}$	0.17	0.69	0.14	30.1	1.15
$PLA^{0.16}_{3.8}$-$PEP^{0.63}_{14.5}$-$PS^{0.21}_{5.5}$	0.16	0.63	0.21	33.1	1.17
$PLA^{0.13}_{3.8}$-$PEP^{0.54}_{14.5}$-$PS^{0.33}_{10.0}$	0.13	0.54	0.33	39.3	1.15
$PLA^{0.12}_{3.8}$-$PEP^{0.48}_{14.5}$-$PS^{0.40}_{14.2}$	0.12	0.48	0.40	44.9	1.15
$PLA^{0.10}_{3.8}$-$PEP^{0.41}_{14.5}$-$PS^{0.49}_{20.1}$	0.10	0.41	0.49	52.6	1.14
$PLA^{0.08}_{3.8}$-$PEP^{0.33}_{14.5}$-$PS^{0.59}_{30.8}$	0.08	0.33	0.59	66.7	1.15
$PLA^{0.50}_{19.1}$-$PEP^{0.50}_{18.2}$	0.50	0.50	0.00	57.4	1.10
$PLA^{0.43}_{19.1}$-$PEP^{0.43}_{18.2}$-$PS^{0.14}_{7.4}$	0.43	0.43	0.14	66.8	1.19
$PLA^{0.41}_{19.1}$-$PEP^{0.42}_{18.2}$-$PS^{0.17}_{9.1}$	0.41	0.42	0.17	69.0	1.17
$PLA^{0.51}_{37.4}$-$PS^{0.49}_{34.3}$	0.51	0.49	0.00	110.9	1.11
$PLA^{0.43}_{37.4}$-$PEP^{0.42}_{34.3}$-$PS^{0.15}_{15.0}$	0.43	0.42	0.15	130.0	1.18
$PLA^{0.42}_{37.4}$-$PEP^{0.41}_{34.3}$-$PS^{0.18}_{18.5}$	0.42	0.41	0.18	134.4	1.17
$PLA^{0.51}_{48.0}$-$PEP^{0.49}_{43.2}$	0.51	0.49	0.00	141.2	1.12
$PLA^{0.43}_{48.0}$-$PEP^{0.41}_{43.2}$-$PS^{0.17}_{22.5}$	0.43	0.41	0.17	169.8	1.23

[a]Superscripts and subscripts refer to volume fraction f and backbone degree of polymerization N_{bb} calculated using f and M_n. [b]Determined by proton nuclear magnetic resonance (^{1}H NMR) spectroscopy with densities of ρ_{PLA} = 1.154 g/mL, ρ_{PEP} = 0.79 g/mL, and ρ_{PS} = 0.969 g/mL.[39,40] [c]M_n for diblocks was determined by size exclusion chromatography (SEC) with multiangle laser light scattering (MALS) and refractive index (RI) detection using tetrahydrofuran (THF) as the eluent. M_n for triblocks was calculated based on M_n of the parent diblock and the weight fraction of each block (obtained from the volume fraction and density). [d]Determined by SEC with RI detection using THF as the mobile phase.

angle or specimen deformation during sample preparation. Based on Figure 7B, the cylinders correspond to the PS domains, while the undulating layers correspond to PLA domains, both surrounded by a PEP matrix. The RCCUL phase seems to be thermodynamically stable; identical SAXS patterns (Figure S12) were obtained after (*i*) annealing at 150 °C for 24 h, and (*ii*) solvent casting from THF followed by annealing (150 °C, 24 h).

Giant RCCUL Phase. Bottlebrush block polymers readily self-assemble into large mesoscopic morphologies with unit cell parameters exceeding 100 nm.[30] However, these giant morphologies have been limited to the simple LAM and HEX structures in previous studies.[33,45] In the previous section, we demonstrated a series of intriguing morphologies using frustrated PLA-PEP-PS bottlebrush block terpolymers at relatively low molecular weights (N_{bb}(PLA) + N_{bb}(PEP) ≈ 20) leading to unit cell parameters of less than 50 nm. We targeted the RCCUL compositional region (Figure 2) and increased the total molecular weight (or N_{bb}) of the bottlebrushes. Figure 8 presents the SAXS pattern and the TEM image of an RCCUL sample with N_{bb} = 44.7. The RCCUL unit cell parameters are $a = b$ = 62.8 nm. Interestingly, in contrast to the morphologies observed with the low molecular weight specimens (Figures 7 and S13), the minority LAM phase disappears at higher molecular weight (as indicated by SAXS), leaving behind a sample that exclusively exhibits the RCCUL phase; this intriguing phenomenon will be discussed in the following section. Additionally, the principal peak q_{11} is quite weak in the high molecular weight samples (Figures 8 and S14–S15), which may be related to the structure factor. A similar phenomenon was observed in the layered samples (where the first peak disappeared), which is explained by structure factor calculations (see Figures S8–S10). In the TEM image shown in Figure 8B, a pair of narrow light gray stripes appear within the central region of a broader stripe, and the black cylindrical domains occupy a larger volume fraction than that of PS in the

https://doi.org/10.1021/acsnano.4c13416
ACS Nano 2025, 19, 1211–1221

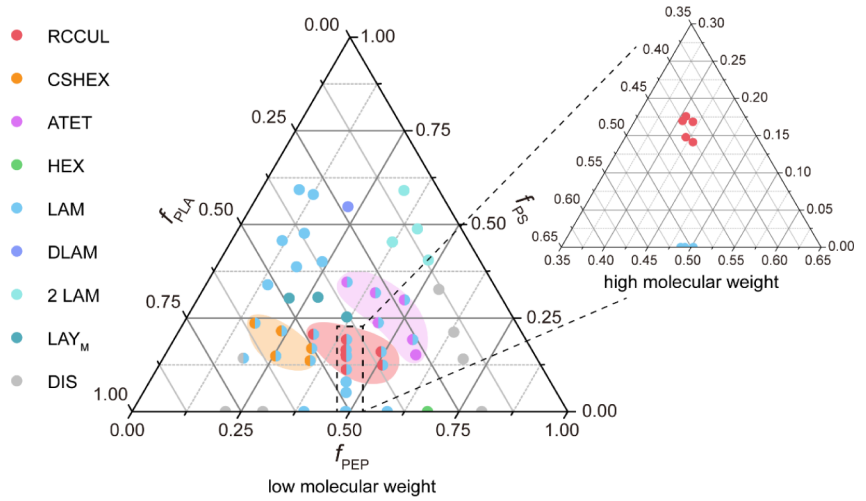

Figure 2. Phase portrait of PLA-PEP-PS bottlebrush block polymers. Bottlebrushes with relatively low molecular weight (N_{bb}(PLA) + N_{bb}(PEP) ≈ 20) are shown in the full phase portrait. Double-color circles indicate samples with coexisting phases indicated by the colors. Shaded regions highlight the three cylinder-containing phases, CSHEX, ATET, and RCCUL. Higher molecular weight sample locations are identified in the expanded phase portrait (top right).

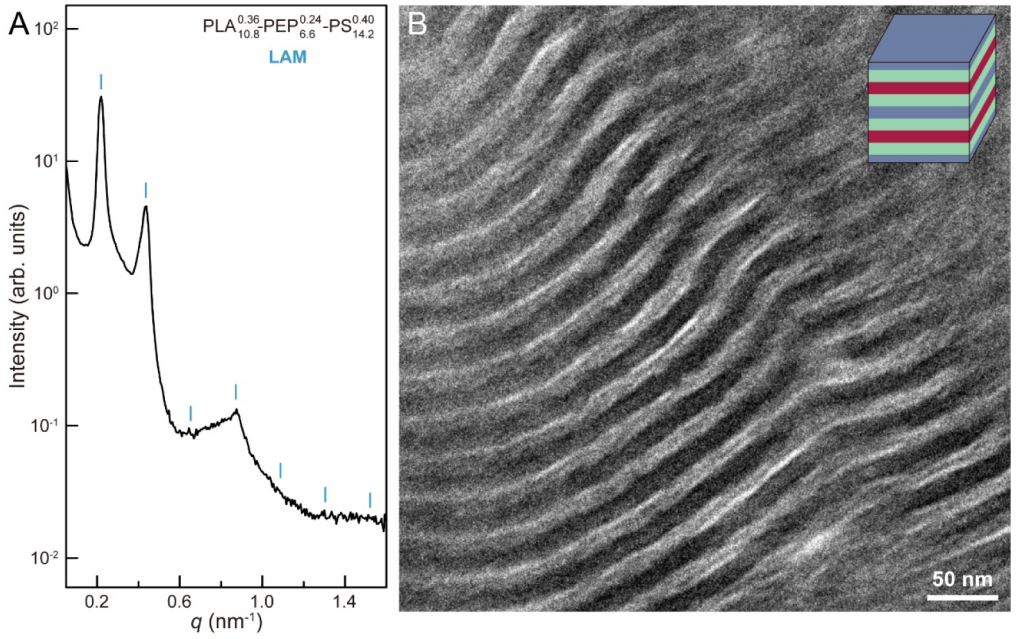

Figure 3. SAXS pattern (A) and TEM image (B) of $PLA^{0.36}_{10.8}$-$PEP^{0.24}_{6.6}$-$PS^{0.40}_{14.2}$ with LAM morphology. The lamellar peaks in the SAXS pattern are identified by the vertical lines. In the TEM image, all three domains, PLA, PEP, and PS are distinguishable, corresponding to gray, white, and black domains, respectively, under the staining of RuO_4 vapor. A three-color LAM scheme is inserted at the top right of (B).

block polymers, where f_{PS} = 0.14. This suggests that the RuO_4 vapor may actually selectively stain the interface between two blocks (PLA/PEP and PEP/PS), consistent with previous reports.[46,47]

We increased the total molecular weight of the PLA-PEP-PS bottlebrush block terpolymers further while keeping the composition in the RCCUL region. For these highest molecular weight samples (N_{bb} > 85), a solvent casting step using THF (0.1 g/mL solution, with natural evaporation until dry, usually overnight) was introduced before annealing, as annealing alone did not result in a well-ordered morphology (Figure S14). The SAXS pattern in Figure S14 indicates that the RCCUL phase is preserved in the high molecular weight sample. A plot of unit cell parameters (a = b) as a function of N_{bb} is shown in Figure 9A, where a ranges from approximately 40 to 133 nm, scaling as $a \sim N_{bb}^{0.74\pm0.02}$ (R^2 = 0.99). We attribute the scaling exponent 0.74, as opposed to 0.8 to 0.9 reported in previous bottlebrush studies,[48,49] to the short side chains (1−2 kg/mol), leading to a relatively flexible conformation. A similar exponent (≈ 0.7) was reported for PS-PEO diblock bottlebrushes with short side chains.[50] Figure 9B shows a TEM image from sample $PLA^{0.43}_{48.0}$-$PEP^{0.41}_{43.2}$-$PS^{0.17}_{22.5}$ with the largest RCCUL structure obtained in this work.

DISCUSSION

In this study, we synthesized a set of frustrated PLA-PEP-PS bottlebrush block terpolymers with well-controlled molecular weight and dispersity by ROMP (Scheme 1, Figure 1, and

https://doi.org/10.1021/acsnano.4c13416
ACS Nano 2025, 19, 1211−1221

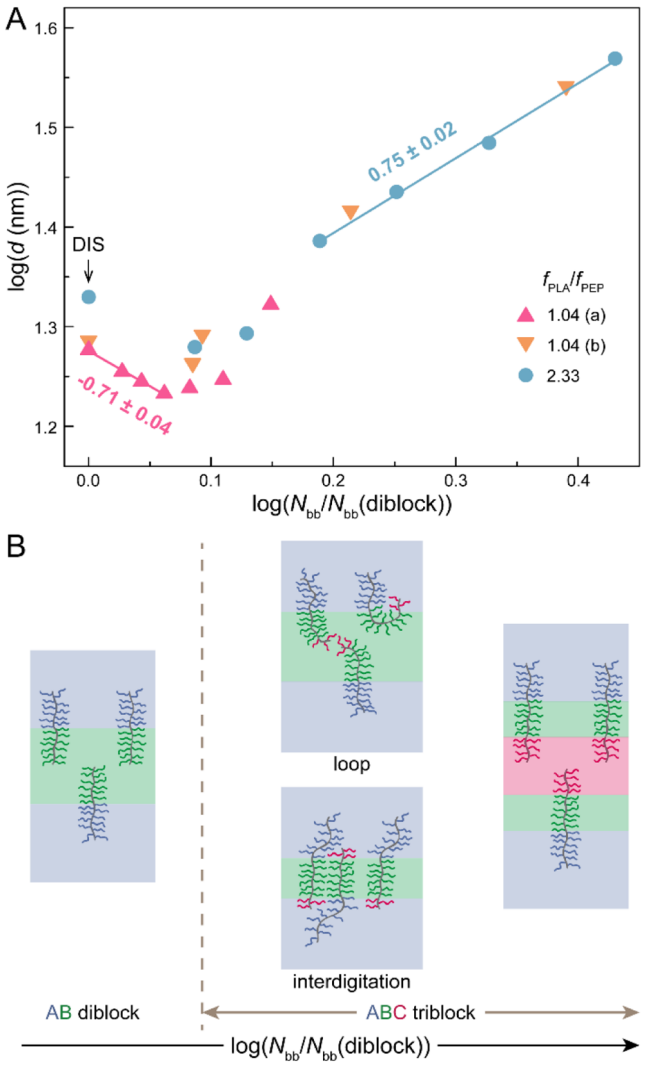

Figure 4. (A) Domain spacing of the layered structure as a function of N_{bb}. The data point for the diblock f_{PLA}/f_{PEP} = 2.33 and N_{bb}/N_{bb}(diblock) = 1 (vertical arrow) corresponds to a disordered phase. The data were extracted from three batches of the bottlebrush block terpolymers with parent diblocks $PLA^{0.51}_{10.3}$-$PEP^{0.49}_{8.6}$ (f_{PLA}/f_{PEP} = 1.04(a)), $PLA^{0.51}_{10.3}$-$PEP^{0.49}_{9.3}$ (f_{PLA}/f_{PEP} = 1.04(b)), and $PLA^{0.70}_{13.9}$-$PEP^{0.30}_{5.6}$ (f_{PLA}/f_{PEP} = 2.33), respectively. (B) Sketches of polymer chains (PLA in blue, PEP in green, PS in red) tentatively show how the morphology is assembled.

Table 1). Scanning of the compositional space by SAXS and TEM revealed multiple mesoscopic morphologies, including layered structures (LAM, LAY_M, DLAM, and 2LAM) and three cylinder-containing morphologies (CSHEX, ATET, and RCCUL) (Figures 2−7). Additionally, we have demonstrated the capacity of bottlebrush block polymers to achieve giant complex mesoscopic morphologies, exemplified by the RCCUL, upon increasing the total molecular weight (Figures 8 and 9). The unit cell parameters for the RCCUL phase ranged from 40 to 130 nm and scaled as $a \sim N_{bb}^{0.74\pm0.02}$ (Figure 9).

ABC triblock terpolymers offer great opportunities for generating intriguing structures due to an expansive set of molecular parameters, resulting in unique chain packing arrangements.[51] Chang et al. discovered an atypical decrease in lamellar domain in frustrated PLA-PS-PEO bottlebrush polymers, where $\chi_{PLA\text{-}PS} > \chi_{PS\text{-}PEO} > \chi_{PLA\text{-}PEO}$.[52] They attributed this phenomenon to the unique chain packing resulting from a small (negative) $\chi_{PLA\text{-}PEO}$, leading to mixing of the PEO and PLA blocks, which can reduce the most unfavorable contacts between PLA and PS blocks. Mixing of PEO and PLA consequently caused the polymer to adopt loop and interdigitation conformations. A decrease in the lamellar domain spacing in the low f_{PS} region was also observed in our work, which we similarly attribute to the small interfacial energy between the PLA and PS blocks (Figure 4). The $\chi_{PLA\text{-}PS}$ (≈ 0.078)[53] is close to $\chi_{PEP\text{-}PS}$ (≈ 0.069)[54] but much smaller than $\chi_{PLA\text{-}PEP}$ (≈ 0.437).[39] However, in contrast to previous work, where the domain spacing decreased monotonically with increasing molecular weight, we document an increase in domain spacing with molecular weight in the large f_{PS} region. This difference can be understood based on $\chi_{PLA\text{-}PEO} \leq 0$ versus $\chi_{PLA\text{-}PS} > 0$.[52,53] As a result, the PLA and PEO will always mix, even with increasing molecular weight, while the PLA and PS blocks will separate when the molecular weight reaches a critical value, inducing a bilayer arrangement (Figure 4B). TEM images revealed that the layered structure in the sample containing coexisting phases exhibited a two-color pattern (Figure S13); however, as f_{PS} increased, a three-color layered structure emerged (Figure S6). The transition in conformation, from looping and interdigitation to bilayers, appears to be accompanied by a shift from a two-color to a three-color layered morphology. The packing might support the persistence of lamellae in the moderate f_C region, both in our PLA-PEP-PS system and the previous PLA-PS-PEO system (the lamellar composition extends up to f_C = 0.2).[52] Increasing the total molecular weight enhances the segregation strength (χN), leading to the clean separation of PLA and PS and ultimately causing the disappearance of the two-color structure. This explains why the pure RCCUL phase appears only in higher molecular weight samples.

In addition to the layered structures, three distinct morphologies involving cylinders were found. CSHEX and ATET morphologies have been reported in nonfrustrated and frustrated linear ABC block polymers, based on a combination of experimental and simulation measurements.[55−58] RCCUL, however, represents a new and previously unreported morphology. This morphology closely resembles the so-called knitting pattern, which exhibits the same *c2mm* symmetry.[59] The knitting pattern has been observed in linear frustrated ABC triblock terpolymers with $\chi_{AB} > \chi_{BC} > \chi_{AC}$, as well as in complex architectures such as ABC miktoarm star polymers, all of which facilitate direct contact between the A and C blocks.[59,60] However, in PLA-PEP-PS bottlebrushes, since the interaction between the PLA and PS blocks is not weak enough ($\chi_{PLA\text{-}PS} \approx 0.078 > \chi_{PEP\text{-}PS} \approx 0.069$) to support direct contact, as supported by the absence of a PLA/PS interface in our morphologies observed via TEM imaging, the discrete B domains in the knitting pattern must merge to encircle the C domains. This leads to the C (PS) domains being segmented by the B (PEP) domains into distinct cylindrical structures. Furthermore, the RCCUL phase is present in a lower f_C region compared to the knitting pattern,[22] accommodating the cylindrical curvature. Furthermore, the RCCUL resembles the cylinders-in-undulating-lamellae (CUL, plane group *p*2) phase in nonfrustrated ABC bottlebrushes described in our earlier work.[38] The CUL phase is found in a compositional range where the single *Fddd* network phase appears in the linear counterparts. Similarly, the RCCUL phase may represent a proxy for network phases. In the PLA-PEP-PS bottlebrush

https://doi.org/10.1021/acsnano.4c13416
ACS Nano 2025, 19, 1211−1221

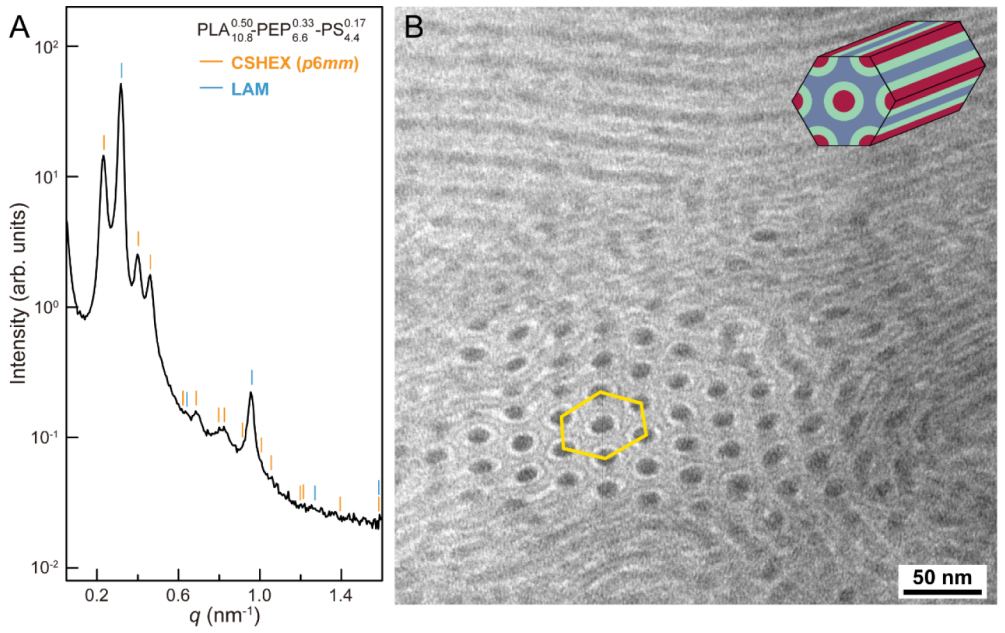

Figure 5. SAXS pattern (A) and TEM image (B) of $PLA^{0.50}_{10.8}$-$PEP^{0.33}_{6.6}$-$PS^{0.17}_{4.4}$ with coexisting CSHEX and LAM morphologies. The SAXS pattern is indexed with a 2D *p6mm* symmetry and a series of LAM peaks, where the indices are identified by vertical lines. In the TEM image, a unit cell is identified by the yellow hexagon. The CSHEX structure is identified at the top right of the TEM image.

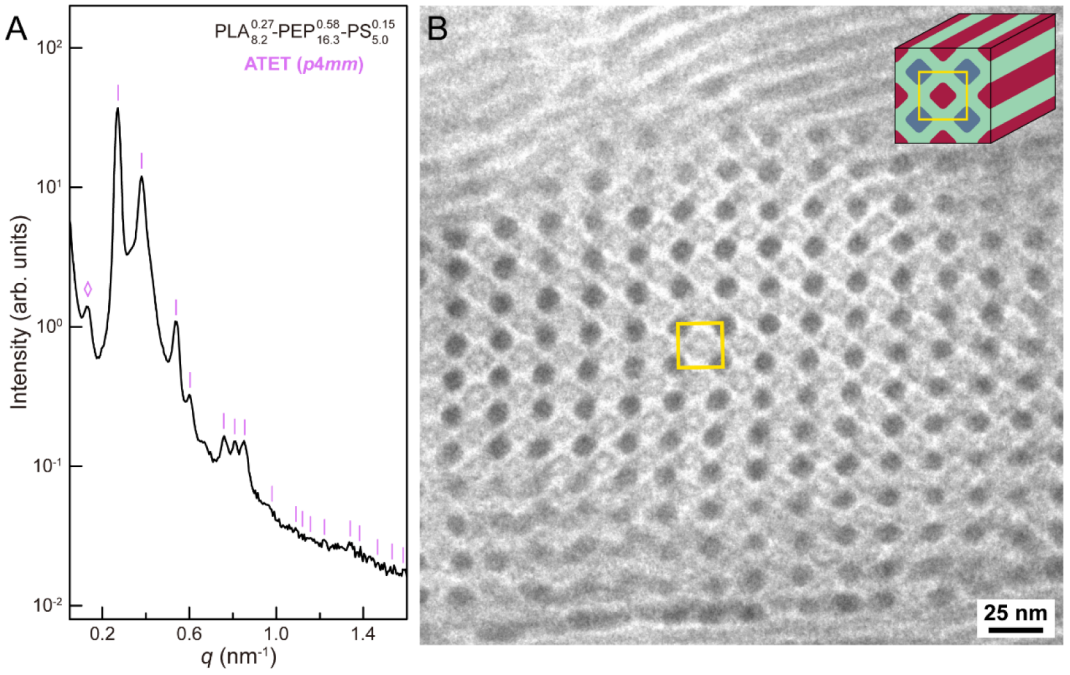

Figure 6. SAXS pattern (A) and TEM image (B) of $PLA^{0.27}_{8.2}$-$PEP^{0.58}_{16.3}$-$PS^{0.15}_{5.0}$ with ATET morphology. The small extra low-*q* peak in (A) (indicated by the hollow diamond) is attributed to the lattice defects (see Figure S11). In (B), a unit cell is identified by the yellow square. An ATET scheme is inserted at the top right of the TEM image.

systems, however, we did not observe any network phases. This contrasts with the nonfrustrated systems, where a core-shell GYR was found, although the alternating GYR and *Fddd* phases were absent.[37] These differences can be better understood by considering the molecular arrangements associated with the linear polymers. In frustrated linear ABC triblock polymers, the network window is narrower than in nonfrustrated systems.[18,61,62] This narrowing is likely due to the pronounced separation at the AB interface, which brings about a more stretched conformation, making it more challenging to accommodate the complex, negative Gauss curvature, interface of the network phase. In frustrated ABC bottlebrushes, the more rigid molecular architecture exacerbates this packing problem, effectively eliminating the network window.

We have demonstrated the potential of ABC bottlebrushes to create large, complex, mesoscopic structures, exemplified by the RCCUL phase. The unit cell parameter of the RCCUL phase can exceed 130 nm (with N_{bb} = 113.7, Figure 9) with straightforward processing, involving solvent casting overnight

https://doi.org/10.1021/acsnano.4c13416
ACS Nano 2025, 19, 1211−1221

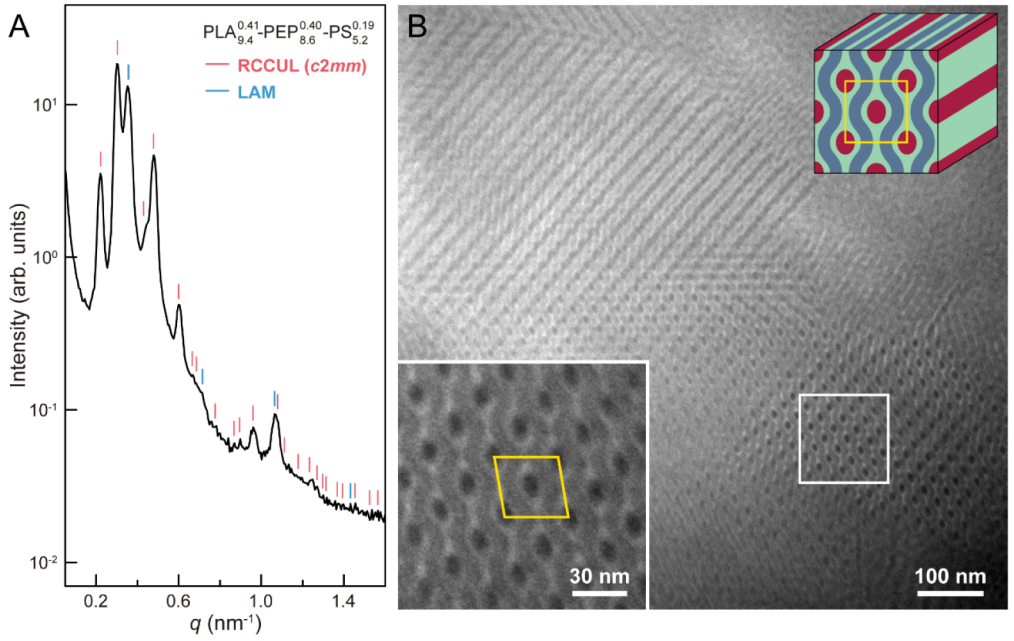

Figure 7. SAXS pattern (A) and TEM image (B) from $PLA_{9.4}^{0.41}$-$PEP_{8.6}^{0.40}$-$PS_{5.2}^{0.19}$ with coexisting RCCUL and LAM morphologies. In the TEM image, a magnified version of the squared region is inserted at the bottom left, where a unit cell is identified by the yellow parallelogram. An RCCUL scheme is inserted at the top right of the TEM image.

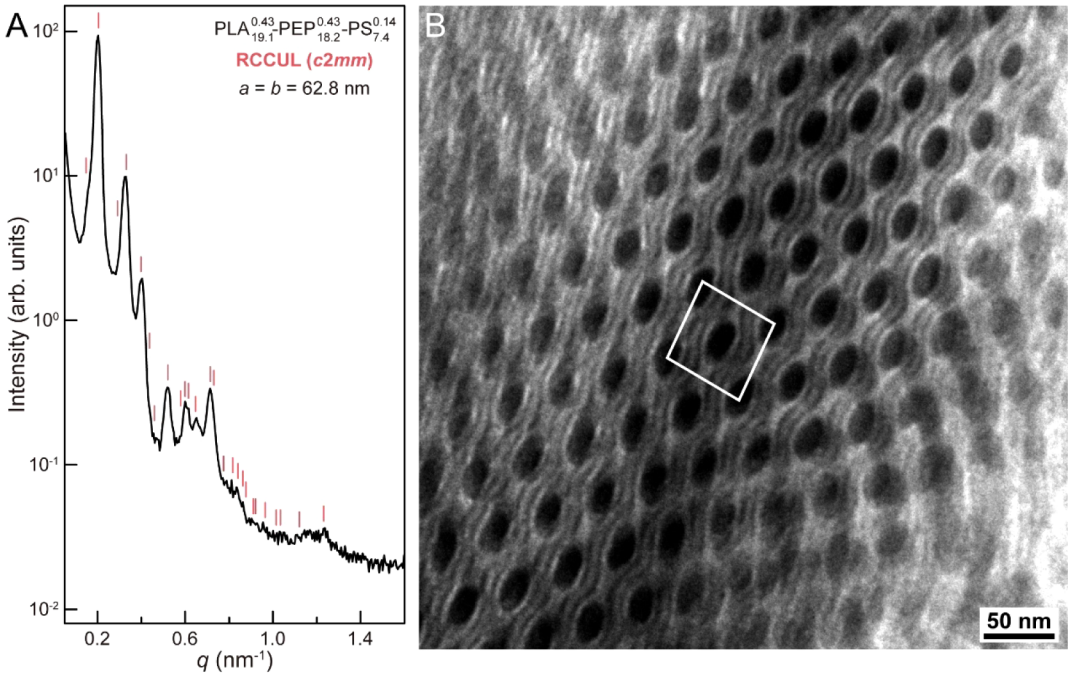

Figure 8. SAXS pattern (A) and TEM image (B) of $PLA_{19.1}^{0.43}$-$PEP_{18.2}^{0.43}$-$PS_{7.4}^{0.14}$ with pure RCCUL. A unit cell is identified by the white parallelogram in (B).

followed by annealing at 150 °C for 24 h. In linear systems, achieving morphologies with feature sizes greater than 100 nm is challenging and typically requires extended casting times. For instance, obtaining a GYR structure with a unit cell parameter of 258 nm (using a diblock copolymer with a molecular weight of 750 kg/mol) required a two-week casting process.[63] Our work reveals that the bottlebrush architecture significantly accelerates ordering kinetics, readily producing complex structures with large dimensions, extending beyond simple phases such as LAM and HEX.

CONCLUSION

In this study, a library of frustrated bottlebrush block terpolymers, PLA-PEP-PS, spanning wide regions of composition and molecular weight space was synthesized by ROMP. Several mesoscopic morphologies, including the layered structures CSHEX, ATET, and RCCUL, were revealed by the combination of SAXS and TEM. An atypical non-monotonic trend in lamellar domain spacing with overall molecular weight was documented and ascribed to a molecular packing transition from looping and interdigitation to a bilayer

https://doi.org/10.1021/acsnano.4c13416
ACS Nano 2025, 19, 1211−1221

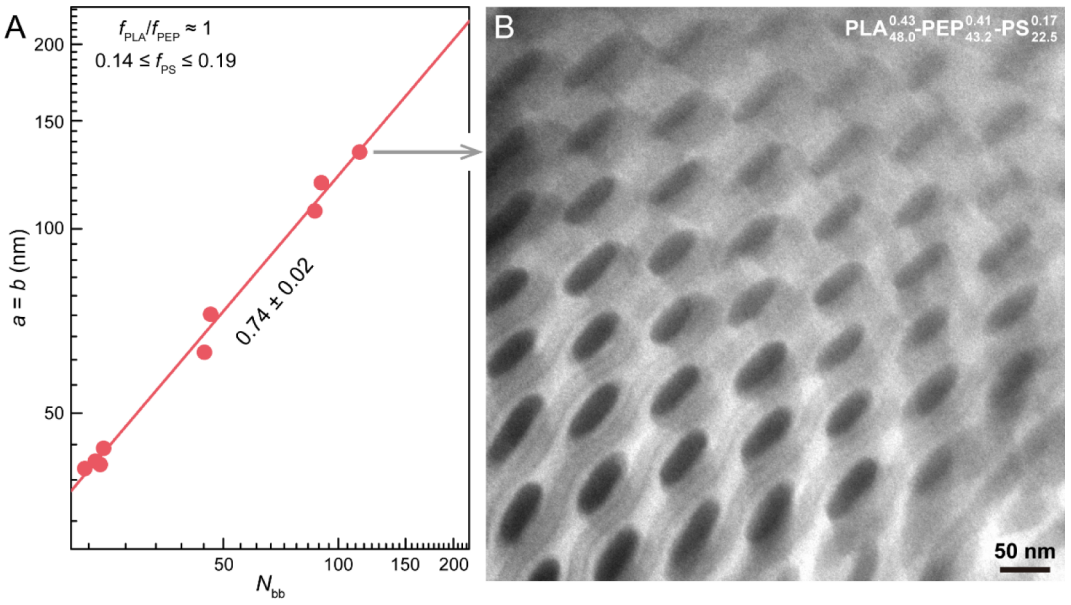

Figure 9. (A) Unit cell parameters (based on SAXS) of the RCCUL phase as a function of N_{bb}. (B) TEM image from sample $PLA^{0.43}_{48.0}$-$PEP^{0.41}_{43.2}$-$PS^{0.17}_{22.5}$ with the unit cell parameters ($a = b$) of 133.3 nm.

arrangement, accompanied by a two-color to three-color morphology transition. Giant RCCUL unit cell dimensions up to 130 nm were achieved in high molecular weight specimens using a straightforward processing method: solvent casting overnight followed by thermal annealing at 150 °C for 24 h. This process is significantly simpler than the methods used for high molecular weight linear polymers. Our findings highlight that bottlebrush block polymers can be used to create new morphologies with a broad range of dimensions. This versatility is likely to facilitate the application of bottlebrush polymers across numerous fields.

EXPERIMENTAL METHODS

Synthesis and Chemical Characterizations. AB diblock bottlebrush copolymers PLA-PEP and ABC triblock bottlebrush terpolymers PLA-PEP-PS were prepared by sequential ring-opening metathesis polymerization (ROMP) of norbornene-functionalized macromonomers, PLA (MM_A, M_n = 1780 g/mol, $Đ$ = 1.13), PEP (MM_P, M_n = 1290 g/mol, $Đ$ = 1.11), and PS (MM_S, M_n = 1240 g/mol, $Đ$ = 1.14), catalyzed by Grubbs third catalyst (G3, synthesized from Grubbs second catalyst bought from Sigma-Aldrich) in anhydrous dichloromethane (DCM). Particular details of the polymer synthesis and characterizations were reported in our previous publications.[37,38] A series of child ABC triblock terpolymers along an isopleth with constant f_{PEP}/f_{PS} but different f_{PLA} in the ternary phase portrait were efficiently synthesized by extending a parent PLA-PEP diblock with the PS block.

The M_n of macromonomers and f_i, for each block of the bottlebrushes were characterized using proton nuclear magnetic resonance (^{1}H NMR) spectroscopy with $CDCl_3$ as the solvent on a Bruker Avance III HD nanobay AX-400 spectrometer (400 MHz) with a 60-slot SampleXpress autosampler. The dispersity, $Đ$, of all polymers was measured by size exclusion chromatography (SEC) with a refractive index (RI) detector and tetrahydrofuran (THF) as the mobile phase (room temperature, 1.0 mL/min). M_n for each ABC triblock was calculated based on f_i of each block and M_n of its parent diblock, which was measured by SEC using a Wyatt Technology DAWN Heleos II multiangle laser light scattering (MALS) detector with 658 nm wavelength and a Wyatt OPTILAB T-rEX RI detector (THF, 1.0 mL/min, 25 °C). The refractive index increment (dn/dc) for the diblock bottlebrushes was determined by SEC assuming 100% mass recovery.

Differential Scanning Calorimetry (DSC). DSC measurements were carried out on a TA Instrument Q1000. Approximately 5 mg of the sample was loaded into hermetically sealed aluminum Tzero DSC pans (DSC Consumables, Austin, MN). Samples were first cooled to −120 °C and then heated to 150 °C to erase thermal history. Then the sample was cooled to −120 °C again and reheated to 150 °C at 10 °C/min. Data collected on the second heating were used for the analysis.

Small-Angle X-ray Scattering (SAXS). SAXS data were predominantly collected at the Characterization Facility, University of Minnesota, using a Xenocs Ganesha instrument equipped with a four-position INSTEC heating stage. Additional experiments were conducted at the Materials Research Laboratory (MRL), BioPACIFIC Materials Innovation Platform of the National Science Foundation, University of California, Santa Barbara, using a custom-built SAXS diffractometer, and at the Brookhaven National Laboratory utilizing synchrotron SAXS. Unless noted, bulk samples were annealed under vacuum at 150 °C for 24 h before measurement. During the measurements, each sample was first equilibrated at a target temperature (usually 80 °C) for 10 min.

Transmission Electron Microscopy (TEM). TEM images were obtained on an FEI Tecnai Spirit Bio-Twin TEM with an accelerating voltage of 120 kV. Polymer samples were loaded in a DSC pan and annealed at 150 °C under vacuum for 24 h then cooled to 80 °C for additional annealing for 2 h. Then, samples were cryo-sectioned using Leica EM UC6 ultramicrotome with a Diatome diamond knife and placed on 400-mesh copper grids. Ultrathin sections (~70 nm) were stained with the vapor from freshly prepared RuO_4 solutions for 4 min, leading to unstained PEP domains (white), slightly stained PLA domains (gray), and strongly stained PS domains (black).

ASSOCIATED CONTENT

Supporting Information

The Supporting Information is available free of charge at https://pubs.acs.org/doi/10.1021/acsnano.4c13416.

Detailed synthesized route and characterization, ^{1}H NMR spectra, SEC traces, DSC traces, SAXS patterns, TEM images, and calculated scattering results (PDF)

https://doi.org/10.1021/acsnano.4c13416
ACS Nano 2025, 19, 1211−1221

AUTHOR INFORMATION

Corresponding Authors

Frank S. Bates − *Department of Chemical Engineering and Materials Science, University of Minnesota, Minneapolis, Minnesota 55455, United States;* orcid.org/0000-0003-3977-1278; Email: bates001@umn.edu

Timothy P. Lodge − *Department of Chemistry and Department of Chemical Engineering and Materials Science, University of Minnesota, Minneapolis, Minnesota 55455, United States;* orcid.org/0000-0001-5916-8834; Email: lodge@umn.edu

Authors

Shuquan Cui − *Department of Chemistry, University of Minnesota, Minneapolis, Minnesota 55455, United States;* orcid.org/0000-0002-8764-0718

Elizabeth A. Murphy − *Materials Research Laboratory and Department of Chemistry and Biochemistry, University of California, Santa Barbara, California 93106, United States;* orcid.org/0000-0003-0846-7943

Subrata Santra − *Department of Chemistry, University of Minnesota, Minneapolis, Minnesota 55455, United States*

Complete contact information is available at: https://pubs.acs.org/10.1021/acsnano.4c13416

Notes

The authors declare no competing financial interest.

ACKNOWLEDGMENTS

This work was supported by the National Science Foundation (NSF) through the University of Minnesota MRSEC under Award DMR-2011401. Parts of this work were carried out in the Characterization Facility, University of Minnesota, which receives partial support from the NSF through the MRSEC (Award Number DMR-2011401) and the NNCI (Award Number ECCS-2025124) programs. The research reported here was partially supported by the BioPACIFIC Materials Innovation Platform of the National Science Foundation under Award No. DMR-1933487 (equipment and characterization). This research also used resources from Sector 11-BM CMS beamline of the National Synchrotron Light Source II, a U.S. Department of Energy (DOE) Office of Science User Facility operated for the DOE Office of Science by Brookhaven National Laboratory under Contract no. DE-SC0012704.

REFERENCES

(1) Zhang, J. L.; Yu, X. H.; Yang, P.; Peng, J.; Luo, C. X.; Huang, W. H.; Han, Y. C. Microphase Separation of Block Copolymer Thin Films. *Macromol. Rapid Commun.* **2010**, *31*, 591−608.

(2) Spencer, R. K. W.; Matsen, M. W. Domain Bridging in Thermoplastic Elastomers of Star Block Copolymer. *Macromolecules* **2017**, *50*, 1681−1687.

(3) Steube, M.; Johann, T.; Barent, R. D.; Mueller, A. H. E.; Frey, H. Rational Design of Tapered Multiblock Copolymers for Thermoplastic Elastomers. *Prog. Polym. Sci.* **2022**, *124*, 101488.

(4) He, H.; Rahimi, K.; Zhong, M. J.; Mourran, A.; Luebke, D. R.; Nulwala, H. B.; Möller, M.; Matyjaszewski, K. Cubosomes from Hierarchical Self-Assembly of Poly(ionic liquid) Block Copolymers. *Nat. Commun.* **2017**, *8*, 14057.

(5) Ha, S.; La, Y.; Kim, K. T. Polymer Cubosomes: Infinite Cubic Mazes and Possibilities. *Acc. Chem. Res.* **2020**, *53*, 620−631.

(6) Maekawa, S.; Seshimo, T.; Dazai, T.; Sato, K.; Hatakeyama-Sato, K.; Nabae, Y.; Hayakawa, T. Chemically Tailored Block Copolymers for Highly Reliable Sub-10-nm Patterns by Directed Self-Assembly. *Nat. Commun.* **2024**, *15*, 5671.

(7) Qiao, L.; Vega, D. A.; Schmid, F. Stability and Elasticity of Ultrathin Sphere-Patterned Block Copolymer Films. *Macromolecules* **2024**, *57*, 4629−4634.

(8) Zhao, D. Y.; Feng, J. L.; Huo, Q. S.; Melosh, N.; Fredrickson, G. H.; Chmelka, B. F.; Stucky, G. D. Triblock Copolymer Syntheses of Mesoporous Silica with Periodic 50 to 300 Angstrom Pores. *Science* **1998**, *279*, 548−552.

(9) Dorin, R. M.; Sai, H.; Wiesner, U. Hierarchically Porous Materials from Block Copolymers. *Chem. Mater.* **2014**, *26*, 339−347.

(10) Xiang, L.; Li, Q.; Li, C.; Yang, Q. Q.; Xu, F. G.; Mai, Y. Y. Block Copolymer Self-Assembly Directed Synthesis of Porous Materials with Ordered Bicontinuous Structures and Their Potential Applications. *Adv. Mater.* **2023**, *35*, 2207684.

(11) Bates, F. S.; Hillmyer, M. A.; Lodge, T. P.; Bates, C. M.; Delaney, K. T.; Fredrickson, G. H. Multiblock Polymers: Panacea or Pandora's Box? *Science* **2012**, *336*, 434−440.

(12) Lodge, T. P. Block Copolymers: Past Successes and Future Challenges. *Macromol. Chem. Phys.* **2003**, *204*, 265−273.

(13) Mai, Y. Y.; Eisenberg, A. Self-Assembly of Block Copolymers. *Chem. Soc. Rev.* **2012**, *41*, 5969−5985.

(14) Bates, F. S.; Fredrickson, G. H. Block Copolymers—Designer Soft Materials. *Phys. Today* **1999**, *52*, 32−38.

(15) Zheng, W.; Wang, Z. G. Morphology of ABC Triblock Copolymers. *Macromolecules* **1995**, *28*, 7215−7223.

(16) Chang, A. B.; Bates, F. S. The ABCs of Block Polymers. *Macromolecules* **2020**, *53*, 2765−2768.

(17) Li, L. Y.; Xu, Z. W.; Li, W. H. Emergence of Connected Binary Spherical Structures from the Self-assembly of an AB_2C Four-Arm Star Terpolymer. *Macromolecules* **2022**, *55*, 9890−9899.

(18) Tyler, C. A.; Qin, J.; Bates, F. S.; Morse, D. C. SCFT Study of Nonfrustrated ABC Triblock Copolymer Melts. *Macromolecules* **2007**, *40*, 4654−4668.

(19) Chatterjee, J.; Jain, S.; Bates, F. S. Comprehensive Phase Behavior of Poly(isoprene-b-styrene-b-ethylene oxide) Triblock Copolymers. *Macromolecules* **2007**, *40*, 2882−2896.

(20) Auschra, C.; Stadler, R. New Ordered Morphologies in ABC Triblock Copolymers. *Macromolecules* **1993**, *26*, 2171−2174.

(21) Stadler, R.; Auschra, C.; Beckmann, J.; Krappe, U.; Voight-Martin, I.; Leibler, L. Morphology and Thermodynamics of Symmetric Poly(A-block-B-block-C) Triblock Copolymers. *Macromolecules* **1995**, *28*, 3080−3097.

(22) Liu, M.; Li, W.; Qiu, F.; Shi, A.-C. Theoretical Study of Phase Behavior of Frustrated ABC Linear Triblock Copolymers. *Macromolecules* **2012**, *45*, 9522−9530.

(23) Verduzco, R.; Li, X.; Pesek, S. L.; Stein, G. E. Structure, function, Self-Assembly, and Applications of Bottlebrush Copolymers. *Chem. Soc. Rev.* **2015**, *44*, 2405−2420.

(24) Li, Z.; Tang, M.; Liang, S.; Zhang, M.; Biesold, G. M.; He, Y.; Hao, S.-M.; Choi, W.; Liu, Y.; Peng, J.; Lin, Z. Bottlebrush Polymers: From Controlled Synthesis, Self-Assembly, Properties to Applications. *Prog. Polym. Sci.* **2021**, *116*, 101387.

(25) Karavolias, M. G.; Elder, J. B.; Ness, E. M.; Mahanthappa, M. K. Order-to-Disorder Transitions in Lamellar Melt Self-Assembled Core−Shell Bottlebrush Polymers. *ACS Macro Lett.* **2019**, *8*, 1617−1622.

(26) Liang, R.; Xue, Y.; Fu, X.; Le, A. N.; Song, Q.; Qiang, Y.; Xie, Q.; Dong, R.; Sun, Z.; Osuji, C. O.; Johnson, J. A.; Li, W.; Zhong, M. Hierarchically Engineered Nanostructures from Compositionally Anisotropic Molecular Building Blocks. *Nat. Mater.* **2022**, *21*, 1434−1440.

(27) Sun, Z.; Liu, R.; Su, T.; Huang, H.; Kawamoto, K.; Liang, R.; Liu, B.; Zhong, M.; Alexander-Katz, A.; Ross, C. A.; Johnson, J. A. Emergence of Layered Nanoscale Mesh Networks through Intrinsic Molecular Confinement Self-Assembly. *Nat. Nanotechnol.* **2023**, *18*, 273−280.

(28) Fei, H.-F.; Yavitt, B. M.; Nuguri, S.; Yu, Y.-G.; Watkins, J. J. Ultrafast Self-Assembly of Bottlebrush Statistical Copolymers: Well-

Ordered Nanostructures from One-Pot Polymerizations. *Macromolecules* **2021**, *54*, 10943−10950.
(29) Xia, Y.; Olsen, B. D.; Kornfield, J. A.; Grubbs, R. H. Efficient Synthesis of Narrowly Dispersed Brush Copolymers and Study of Their Assemblies: The Importance of Side Chain Arrangement. *J. Am. Chem. Soc.* **2009**, *131*, 18525−18532.
(30) Dalsin, S. J.; Rions-Maehren, T. G.; Beam, M. D.; Bates, F. S.; Hillmyer, M. A.; Matsen, M. W. Bottlebrush Block Polymers: Quantitative Theory and Experiments. *ACS Nano* **2015**, *9*, 12233−12245.
(31) Kim, H.-C.; Park, S.-M.; Hinsberg, W. D. Block Copolymer Based Nanostructures: Materials, Processes, and Applications to Electronics. *Chem. Rev.* **2010**, *110*, 146−177.
(32) Daniel, W. F. M.; Burdyńska, J.; Vatankhah-Varnoosfaderani, M.; Matyjaszewski, K.; Paturej, J.; Rubinstein, M.; Dobrynin, A. V.; Sheiko, S. S. Solvent-free, supersoft and superelastic bottlebrush melts and networks. *Nat. Mater.* **2016**, *15*, 183−189.
(33) Rzayev, J. Synthesis of Polystyrene−Polylactide Bottlebrush Block Copolymers and Their Melt Self-Assembly into Large Domain Nanostructures. *Macromolecules* **2009**, *42*, 2135−2141.
(34) Liberman-Martin, A. L.; Chang, A. B.; Chu, C. K.; Siddique, R. H.; Lee, B.; Grubbs, R. H. Processing Effects on the Self-Assembly of Brush Block Polymer Photonic Crystals. *ACS Macro Lett.* **2021**, *10*, 1480−1486.
(35) Gai, Y.; Song, D.-P.; Yavitt, B. M.; Watkins, J. J. Polystyrene-block-poly(ethylene oxide) Bottlebrush Block Copolymer Morphology Transitions: Influence of Side Chain Length and Volume Fraction. *Macromolecules* **2017**, *50*, 1503−1511.
(36) Jiang, L.; Nykypanchuk, D.; Pastore, V. J.; Rzayev, J. Morphological Behavior of Compositionally Gradient Polystyrene−Polylactide Bottlebrush Copolymers. *Macromolecules* **2019**, *52*, 8217−8226.
(37) Cui, S.; Zhang, B.; Shen, L.; Bates, F. S.; Lodge, T. P. Core−Shell Gyroid in ABC Bottlebrush Block Terpolymers. *J. Am. Chem. Soc.* **2022**, *144*, 21719−21727.
(38) Cui, S.; Murphy, E. A.; Zhang, W.; Zografos, A.; Shen, L.; Bates, F. S.; Lodge, T. P. Cylinders-in-Undulating-Lamellae Morphology from ABC Bottlebrush Block Terpolymers. *J. Am. Chem. Soc.* **2024**, *146*, 6796−6805.
(39) Schmidt, S. C.; Hillmyer, M. A. Morphological Behavior of Model Poly(ethylene-alt-propylene)-b-polylactide Diblock Copolymers. *J. Polym. Sci., Part B: Polym. Phys.* **2002**, *40*, 2364−2376.
(40) Epps, T. H.; Cochran, E. W.; Bailey, T. S.; Waletzko, R. S.; Hardy, C. M.; Bates, F. S. Ordered Network Phases in Linear Poly(isoprene-b-styrene-b-ethylene oxide) Triblock Copolymers. *Macromolecules* **2004**, *37*, 8325−8341.
(41) Matsen, M. W.; Beardsley, T. M.; Willis, J. D. Fluctuation-Corrected Phase Diagrams for Diblock Copolymer Melts. *Phys. Rev. Lett.* **2023**, *130*, 248101.
(42) Choo, Y.; Mahajan, L. H.; Gopinadhan, M.; Ndaya, D.; Deshmukh, P.; Kasi, R. M.; Osuji, C. O. Phase Behavior of Polylactide-Based Liquid Crystalline Brushlike Block Copolymers. *Macromolecules* **2015**, *48*, 8315−8322.
(43) Liberman, L.; Coughlin, M. L.; Weigand, S.; Bates, F. S.; Lodge, T. P. Phase Behavior of Linear-Bottlebrush Block Polymers. *Macromolecules* **2022**, *55*, 2821−2831.
(44) Liberman, L.; Coughlin, M. L.; Weigand, S.; Edmund, J.; Bates, F. S.; Lodge, T. P. Impact of Side-Chain Length on the Self-Assembly of Linear-Bottlebrush Diblock Copolymers. *Macromolecules* **2022**, *55*, 4947−4955.
(45) Runge, M. B.; Bowden, N. B. Synthesis of High Molecular Weight Comb Block Copolymers and Their Assembly into Ordered Morphologies in the Solid State. *J. Am. Chem. Soc.* **2007**, *129*, 10551−10560.
(46) Wang, Y.; Coombs, N.; Turak, A.; Lu, Z.-H.; Manners, I.; Winnik, M. A. Interfacial Staining of a Phase-Separated Block Copolymer with Ruthenium Tetroxide. *Macromolecules* **2007**, *40*, 1594−1597.
(47) Libera, M. R.; Egerton, R. F. Advances in the Transmission Electron Microscopy of Polymers. *Polym. Rev.* **2010**, *50*, 321−339.
(48) Gu, W.; Huh, J.; Hong, S. W.; Sveinbjornsson, B. R.; Park, C.; Grubbs, R. H.; Russell, T. P. Self-Assembly of Symmetric Brush Diblock Copolymers. *ACS Nano* **2013**, *7*, 2551−2558.
(49) Lin, T.-P.; Chang, A. B.; Luo, S.-X. L.; Chen, H.-Y.; Lee, B.; Grubbs, R. H. Effects of Grafting Density on Block Polymer Self-Assembly: From Linear to Bottlebrush. *ACS Nano* **2017**, *11*, 11632−11641.
(50) Zhang, B.; Cui, S.; Lodge, T. P.; Bates, F. S. Structure and Phase Behavior of Bottlebrush Diblock Copolymer-Linear Homopolymer Ternary Blends. *Macromolecules* **2023**, *56*, 1663−1673.
(51) Tang, P.; Qiu, F.; Zhang, H. D.; Yang, Y. L. Morphology and Phase Diagram of Complex Block Copolymers: ABC Linear Triblock Copolymers. *Phys. Rev. E* **2004**, *69*, 031803.
(52) Chang, A. B.; Bates, C. M.; Lee, B.; Garland, C. M.; Jones, S. C.; Spencer, R. K. W.; Matsen, M. W.; Grubbs, R. H. Manipulating the ABCs of Self-Assembly via Low-χ Block Polymer Design. *Proc. Natl. Acad. Sci. U. S. A.* **2017**, *114*, 6462−6467.
(53) Sinturel, C.; Bates, F. S.; Hillmyer, M. A. High χ−Low N Block Polymers: How Far Can We Go? *ACS Macro Lett.* **2015**, *4*, 1044−1050.
(54) Sakurai, S.; Hashimoto, T.; Fetters, L. J. Morphology of Polystyrene-block-poly(ethylene-alt-propylene) Diblock Copolymers in the Strong-Segregation Limit. *Macromolecules* **1995**, *28*, 7947−7949.
(55) Mogi, Y.; Nomura, M.; Kotsuji, H.; Ohnishi, K.; Matsushita, Y.; Noda, I. Superlattice Structures in Morphologies of the ABC Triblock Copolymers. *Macromolecules* **1994**, *27*, 6755−6760.
(56) Nagpal, U.; Detcheverry, F. A.; Nealey, P. F.; de Pablo, J. J. Morphologies of Linear Triblock Copolymers from Monte Carlo Simulations. *Macromolecules* **2011**, *44*, 5490−5497.
(57) Radlauer, M. R.; Sinturel, C.; Asai, Y.; Arora, A.; Bates, F. S.; Dorfman, K. D.; Hillmyer, M. A. Morphological Consequences of Frustration in ABC Triblock Polymers. *Macromolecules* **2017**, *50*, 446−458.
(58) Li, L. Y.; Li, W. H. Effect of Branching Architecture on the Self-Assembly of Symmetric ABC-type Block Terpolymers. *Giant* **2021**, *7*, 100065.
(59) Breiner, U.; Krappe, U.; Thomas, E. L.; Stadler, R. Structural Characterization of the "Knitting Pattern" in Polystyrene-block-poly(ethylene-co-butylene)-block-poly(methyl methacrylate) Triblock Copolymers. *Macromolecules* **1998**, *31*, 135−141.
(60) Li, L. Y.; Dong, Q. S.; Li, W. H. Stabilize Various Novel Network Structures via the Alternate Arrangement of A/C Domains in Close Contact by Tailoring ABC Miktoarm Star Architectures. *Macromolecules* **2024**, *57*, 409−419.
(61) Bailey, T. S.; Hardy, C. M.; Epps, T. H.; Bates, F. S. A Noncubic Triply Periodic Network Morphology in Poly(isoprene-b-styrene-b-ethylene oxide) Triblock Copolymers. *Macromolecules* **2002**, *35*, 7007−7017.
(62) You, X. T.; Liu, M. J.; Dong, Q. S.; Li, W. H. Stability of Hierarchical Gyroid Structures in Frustrated ABC Triblock Copolymers. *Macromolecules* **2023**, *56*, 8157−8167.
(63) Urbas, A. M.; Maldovan, M.; DeRege, P.; Thomas, E. L. Bicontinuous Cubic Block Copolymer Photonic Crystals. *Adv. Mater.* **2002**, *14*, 1850−1853.

https://doi.org/10.1021/acsnano.4c13416
ACS Nano 2025, 19, 1211−1221